Molecular Therapy
Nucleic Acids
Original Article

# MicroRNA-466 and microRNA-200 increase endothelial permeability in hyperglycemia by targeting Claudin-5

Marisa Kujawa,[1,3] Megan O'Meara,[1,3] Hainan Li,[1,3] Liping Xu,[1] Sai Pranathi Meda Venkata,[1] Huong Nguyen,[1] Morgan Minjares,[1] Kezhong Zhang,[2] and Jie-Mei Wang[1,2]

[1]Department of Pharmaceutical Sciences, Eugene Applebaum College of Pharmacy and Health Sciences, Wayne State University, Detroit, MI, USA; [2]Centers for Molecular Medicine and Genetics, School of Medicine, Wayne State University, Detroit, MI, USA

**Endothelial cell (EC) permeability is essential to vascular homeostasis in diabetes. MicroRNAs are critical gene regulators whose roles in the EC permeability have yet to be characterized. This study aims to examine the change in cell permeability induced by miR-200 and miR-466 in ECs. Human aortic ECs and dermal microvascular ECs from healthy subjects and type 2 diabetic patients were used. Our *in vitro* experiments unveiled higher expressions of miR-200 family members and miR-466 in diabetic ECs and in healthy ECs when exposed to high glucose. Overexpression of both miR-200 and miR-466 significantly increased EC permeability through transcriptional suppression of Claudin-5, the cell tight junction protein, by directly binding to its 3′ untranslated region. In a mouse model of chronic hyperglycemia mimicking type 2 diabetes in humans (db/db mice), the delayed closure rate of a full-thickness excisional wound was partly rescued by topical application of the miR-200 inhibitor. The topical application of both miR-200 and miR-466 inhibitors exhibited improved efficacy in accelerating wound closure compared with the topical application of miR-200 inhibitor alone. Our study demonstrated the potentially effective approach of miR-200/miR-466 cocktail inhibition to restore vascular integrity and tissue repair in hyperglycemia.**

## INTRODUCTION

Wound healing is a complex process that consists of multiple molecular and cellular activities. It can be divided into three overlapped phases: inflammatory phase, proliferative phase, and remodeling phase.[1] The initial inflammatory response is characterized by the burst of inflammatory cytokines resulting in capillary vasodilatation and leakage.[2] This transient increase of blood flow and vascular permeability not only allows for inflammatory cell infiltration but also facilitates endothelial sprouting from the existing vascular bed, namely angiogenesis. Angiogenesis is a vital process required for the proliferative phase. It is necessary to deliver nutrients and oxygen to the wound, support granulation tissue formation, and reconstruct skin structures. In diabetes, this insufficient angiogenesis fails to produce enough capillaries to maintain critical nutrient supply to tissue deposition. Thus, it results in a chronically unhealed wound, mostly seen in the lower limbs, known as diabetic foot ulcers (DFUs).

DFUs have created a significant socioeconomic burden.[3] Approximately 15% of diabetic patients with DFUs will eventually go through extremity amputation.[4] Multiple factors have contributed to this devastating situation, but one crucial common pathology that occurs early in tissue injury in diabetes is prolonged vascular hyperpermeability. It disturbs the transition from the inflammatory response to the proliferation phase, diminishing angiogenesis and granulation tissue formation,[5] because it causes excessive tissue edema and consequently exacerbates the poor delivery of nutrients and oxygen. This prolonged vascular hyperpermeability has been shown to be attributed to the impaired endothelial barrier function[5,6] because endothelial cells (ECs) are frequently prone to diabetes-related damage such as hyperglycemia, dyslipidemia, and the proinflammatory state.[7] Therefore, understanding how EC barrier function alters under hyperglycemia is critical to developing treatment protocols for wound healing in diabetes.

Tight junctions are important cellular structures crucial to EC permeability.[8] Claudins, occludin, and junctional adhesion molecules constitute approximately 20% of the total junctional proteins in the ECs.[9,10] Claudin-5 is the major claudin expressed in ECs and is considered vital to EC permeability.[11] However, exactly how Claudin-5 is regulated under hyperglycemia remains unknown. Recent investigations targeting dysregulated vascular permeability or angiogenesis using growth factor or cellular interventions have shown promising potential in treating DFUs.[12,13] However, skin wound healing is composed of multiple dynamic processes. Inhibiting/promoting one pathway does not necessarily benefit the whole

Received 29 September 2021; accepted 4 July 2022;
https://doi.org/10.1016/j.omtn.2022.07.002.

[3]These authors contributed equally

**Correspondence:** Jei-Mei Wang, Department of Pharmaceutical Sciences, Eugene Applebaum College of Pharmacy & Health Sciences, Wayne State University, 259 Mack Avenue, 3122 Applebaum Building, Detroit, MI 48201, USA.
**E-mail:** jiemei.wang@wayne.edu

healing process. Therefore, conventional single-molecule or single-cell-type therapies may have limited efficacies on wound healing. It is essential to test molecules that modulate multiple processes involved in wound healing while probing for cocktail therapies. In this regard, microRNAs (miRs) seem to be good candidates.

miRs are small non-coding RNAs, typically 21–25 nt in length.[7] Since its discovery over 30 years ago, the knowledge of miR has been evolving at a fast pace. miRs are now recognized as major players in almost every biological process in eukaryotic organisms, and some are highly conserved across species.[3] In most cases, miRs interact with the 3′ untranslated region (3′ UTR) of target mRNAs to facilitate mRNA degradation and/or to induce translational repression.[14] While numerous studies are investigating miR-mRNA or miR-protein target, relatively few studies of miR-miR interactions or co-actions have been reported. A previous study showed that mouse miR-466(a/b/c/e/p)-3p and miR-200b-3p in kidney collecting duct epithelial cells are tonicity-responsive miRs in high sodium environments.[15] In diabetes, hyperglycemia creates a hypertonic force that draws fluid out of cells and increases vascular permeability, which is already linked with the adverse complications of diabetes.[16] Our previous study showed that both mouse miR-200 and miR-466 families, screened from miR assay, were upregulated in endothelial precursor cells isolated from the mice with type 2 diabetes (T2D).[3] In fact, several reports have shown concomitant alterations of miR-200 and miR-466 families in a number of settings in rodents and humans.[15,17–19] The miR-200 family has five mature miR members in both humans and mice with single-base differences. These five members are expressed from two transcripts that encode the miR-141/miR-200a cluster and the miR-200b/miR-200c/miR-429 cluster, which are located in chromosome 1p36 and chromosome 12p13, respectively[20] (Figure 1C). Furthermore, miR-200 families are upregulated in hyperglycemia,[21] and the therapeutic potential of targeting miR-200 family members, predominantly miR-200b/c, in treating diabetes-related vascular disorders has been tested.[19,22,23] The miR-466 family has one mature miR member in humans, while in mice, it has many single-base different family members. miR-466a/b/c/d/e/f/g/h/I, together with miR-467, miR-669, and miR-297, located in the intron 10 of mouse Sfmbt2 gene, are known as chromosome 2 miR cluster. miR-466 has been reported to participate in the suppression of tumor progression and antiviral defense. However, for both miR-200 and miR-466, it remains unclear whether these two miRs regulate EC permeability.

This study aimed to determine whether miR-200 and miR-466 have a regulatory role in EC permeability and to identify the underlying molecular mechanisms through which miR-466 and miR-200 modulate EC permeability. We also explored the efficacy of cocktail therapy targeting these two miRs in skin wound healing in hyperglycemia. We hypothesized that concurrent upregulation of miR-466 and miR-200 under hyperglycemia increases EC permeability by targeting Claudin-5. Inhibition of these two miRs can restore vascular integrity and pace wound healing. To test this hypothesis, we determined whether high glucose increases miR-466 and miR-200. Next, miR-466 or miR-200 were manipulated to determine whether cell permeability was affected. We also identified Claudin-5 as the direct target of miR-466 and miR-200 in the regulation of cell permeability. In a full-thickness excisional skin wound model, to mimic the skin wound healing in T2D in humans, we used a mouse model of leptin receptor-deficient mice (BKS.Cg-m$^{+/+}$ Lepr$^{db}$/J, db/db) and their healthy littermates (BKS.Cg-m$^{-/-}$ Lep$^{db/-}$ lean, db/+). These animals developed hyperglycemia, obesity, dyslipidemia, and insulin resistance as early as 6–8 weeks of age.[3,24] A full-thickness standard-size excisional wound was created on the dorsal skin. We then tested the impact of miR-466 on wound closure, especially during the early phase of wound healing. The findings from this study provide novel insights into the regulatory roles of miR-466 and miR-200 in endothelial permeability and the dynamic control over the healing course of diabetic skin wounds when miR-466/200 cocktail therapy is implemented.

## RESULTS

### The upregulation of miR-200 and miR-466 increases EC permeability under hyperglycemic conditions

Using a fluorescein isothiocyanate (FITC)-Dextran Transwell assay, we tested the permeability of the monolayer formed by ECs from healthy donors and T2D donors to determine whether hyperglycemia affects EC permeability. Our results showed a higher permeability of diabetic human aortic ECs (HAECs) than healthy HAECs (Figure 1A), suggesting impaired EC layer integrity in diabetic individuals. Some of the healthy ECs were exposed to 25 mM glucose for 72 h before the permeability test. The healthy ECs exposed to endothelial growth media-2 (EGM-2) supplied with 20 mM mannitol and 5 mM glucose served as control. Consistent with our findings in diabetic ECs, high glucose exposure *in vitro* elevated the monolayer permeability of healthy ECs (Figure 1B), replicating the impaired cell function in diabetic ECs. Interestingly, we discovered that miR-466 and miR-200 family members, including miR-200a/b/c, miR-141, and miR-429 (stem-loop structure of each miR containing mature sequences obtained from miRbase.org, Release 22.1, are shown in Figure 1C), were increased in ECs from T2D donors (Figure 1D). To test whether the upregulation is due to the high glucose, healthy ECs were exposed to 25 mM glucose for 72 h to mimic hyperglycemia. The treatment of 20 mM mannitol and 5 mM glucose served as control. We found that the levels of miR-200 family members and miR-466 were increased upon high glucose exposure (Figure 1E). Among miR-200 family members, miR-200b and miR-200c showed the most marked changes. To test whether miR-200 or miR-466 contributes to the increased endothelial permeability, healthy ECs were transfected with miR-200 or miR-466 precursors. Real-time PCR tests have confirmed the upregulation of miR-200 family members or miR-466 upon the precursor transfection (Figure 1F). The results suggest that miR-466 alone drives the increased EC permeability and addition of miR-200 does not lead to any synergistic effect when measuring permeability with the FITC-Dextran Transwell assay.

### Both miR-466 and miR-200 inhibit EC permeability by directly suppressing Claudin-5

Several molecules have shown potential roles in regulating EC permeability, including vascular endothelial (VE)-cadherin (gene symbol

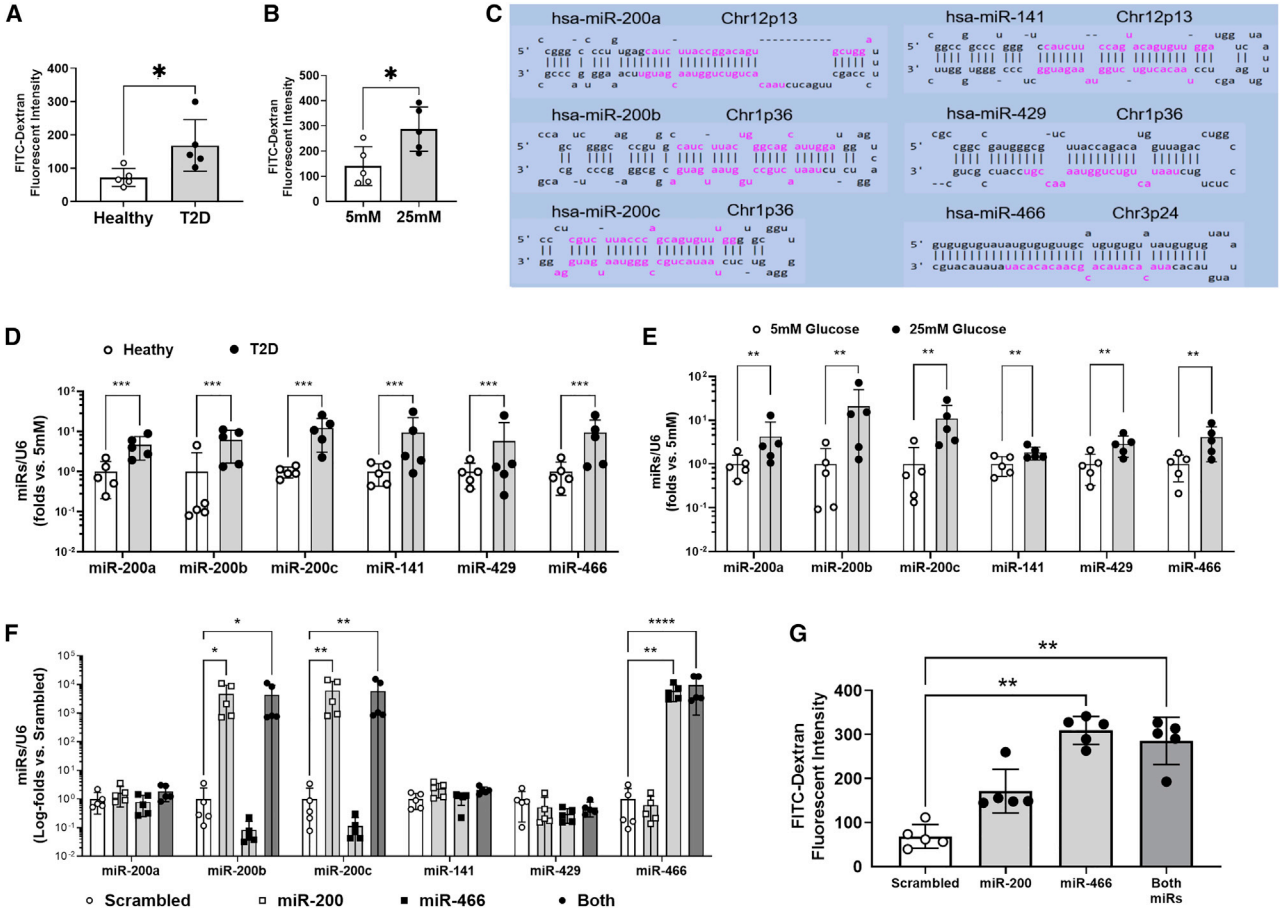


**Figure 1. miR-200 and miR-466 contribute to the increased endothelial cell (EC) permeability in hyperglycemia**

ECs from healthy and type 2 diabetic (T2D) donors were cultured to passage 4–7 before high glucose treatment or gene manipulation. (A) FITC-dextran Transwell assay showing T2D ECs have higher permeability than healthy ECs. n = 5 per group. (B) FITC-dextran Transwell assay showing healthy ECs exposed to 25 mM glucose have higher permeability than control group exposed to 20 mM mannitol and 5 mM glucose. n = 5 per group. (C) Stem-loop structure of miR-466 and miR-200 family, including miR-200a/b/c, miR-141 and miR-429, and miR-466. (D) Real-time quantitative polymerase chain reaction (qPCR) confirmed higher expression levels of miR-200a/b/c, miR-141, miR-429, and miR-466 in T2D ECs than healthy ECs. n = 5 per group. (E) qPCR showing higher expression levels of miR-200a/b/c, miR141, miR-429, and miR-466 in healthy ECs exposed to 25 mM glucose for 72 h compared to the control group exposed to 20 mM mannitol and 5 mM glucose. n = 5 per group. (F) qPCR confirmed the upregulation of miR-200 family members and miR-466 in healthy ECs transfected with miR-200 or miR-466 precursors compared to scrambled controls. n = 5 per group. (G) FITC-dextran Transwell assay indicating increased permeability of healthy ECs transfected with miR-200 or miR-466 precursors is compared to scrambled controls. Data are presented as means ± SDs. *p < 0.05; **p < 0.01; ***p < 0.001; ****p < 0.0001. Mann-Whitney *U* test for statistical analysis (A, B, D, and E); Kruskal-Wallis test, and Mann-Whitney *U* test with Benjamini, Krieger, and Yekutieli's adjustment for multiple comparisons if significant (F and G).

*CDH5*), Connexin43 (gene symbol *GJA1*), and Claudin-5 (gene symbol *CLDN5*), were on both miR-466 and miR-200 target maps based on databases, including Pictar and TargetScan. We detected protein levels of these molecules in HAECs from healthy and T2D donors. Our results indicated that Claudin-5 was significantly increased in ECs from T2D donors, while Connexin43 and VE-cadherin were comparable to HAECs from healthy donors (Figure 2A).

Because human dermal microvascular ECs (HDMECs) were close to the anatomic location of ECs in the skin, we cultured HDMECs and tested their EC permeability and miR changes. Unlike HAECs, diabetic HDMECs possessed modestly lower Claudin-5 protein levels than healthy HDMECs (Figure 2B, p = 0.137). There was a remarkable suppression of Claudin-5 protein levels in healthy ECs transfected with miR-200 or miR-466, but Connexin43 and VE-cadherin were not altered (Figure 3A). The binding details of miR-200 family members and miR-466 on *CLDN5* mRNA are shown in Figure 2C. Using a luciferase reporter carrying *CLDN5* mRNA 3′ UTR, we observed a significant reduction in luciferase activity by the co-transfection of either precursor of miR-200 or miR-466 (Figure 2E). Furthermore, we transfected the healthy HAECs with small interfering RNA (siRNA) against Claudin-5 (*CLDN5* siRNA) before the miR-200 inhibitor or miR-466 inhibitor transfection. The EC permeability assay suggested that the decreased EC permeability induced by

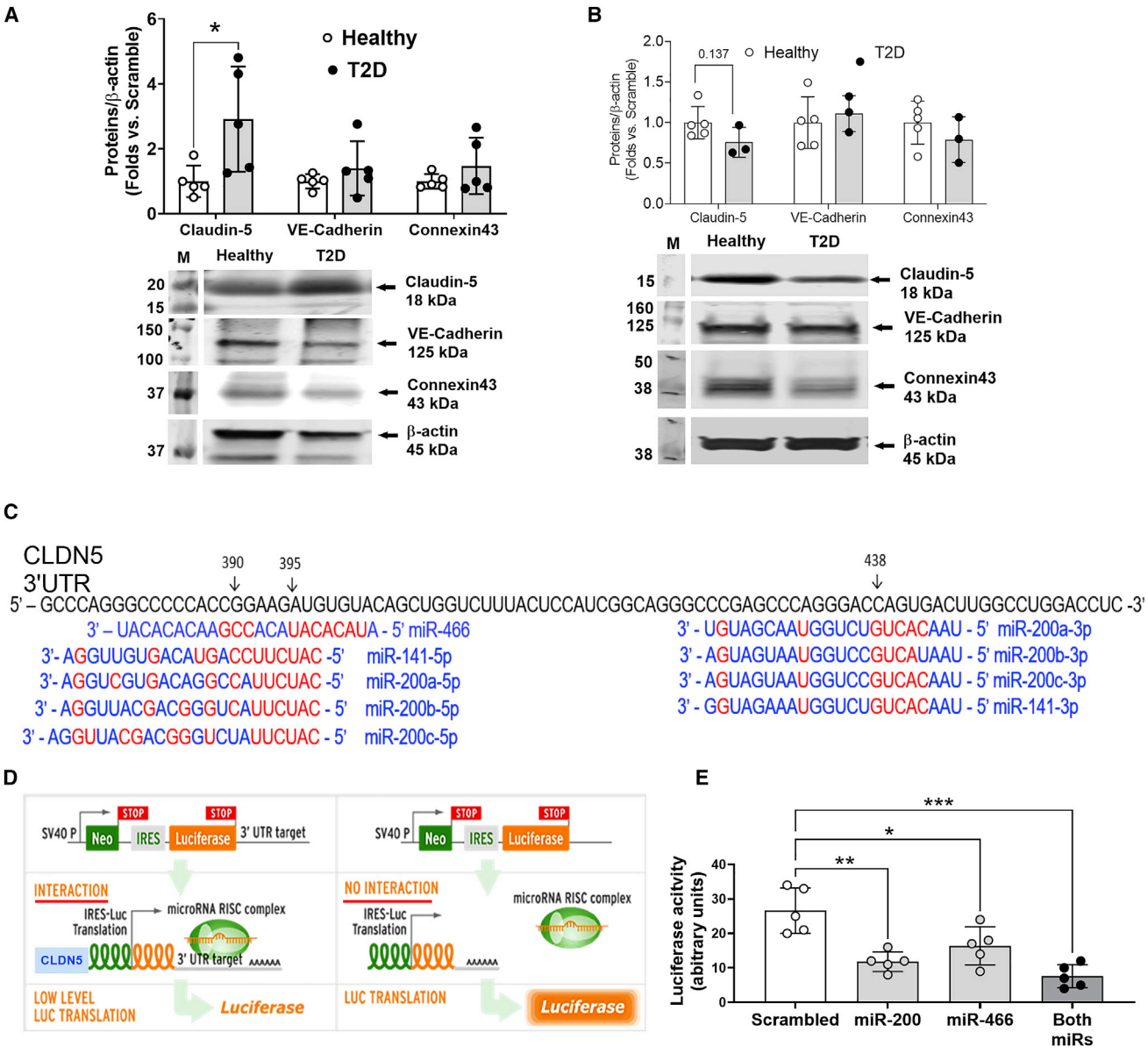


**Figure 2. miR-466 and miR-200 decrease expression level of Claudin-5**

ECs were cultured to passage 4–7 before collection or transfection with miR precursors. (A) Protein expression of Claudin-5, VE-cadherin, and Connexin43 in healthy and T2D human aortic ECs (HAECs). n = 5 per group. Representative bands of western blot are shown below the quantification analysis. (B) Protein expression of Claudin-5, VE-cadherin, and Connexin43 in healthy and T2D human dermal microvascular ECs (HDMECs). n = 3–5 per group. Representative bands of western blot are shown below the quantification analysis. (C) The binding details of miR-200 family, including miR-200a/b/c, miR-141, and miR-466 on *CLDN5* mRNA. (D) Luciferase activity assay illustration of rationale. (E) 3′ UTR luciferase activity assay confirmed reduced luciferase activity in healthy ECs transfected with miR-200 inhibitor or miR-466 inhibitor. Data are presented as means ± SDs. *p < 0.05; **p < 0.01; ***p < 0.001. M, marker. Mann-Whitney *U* test for statistical analysis (A and B); Kruskal-Wallis test and Mann-Whitney *U* test with Benjamini, Krieger, and Yekutieli's adjustment for multiple comparisons if significant (E).

miR-200 or miR-466 inhibition was blunted by knocking down Claudin-5 (Figure 3B). In HDMECs, we found that the EC permeability could be increased by high glucose (25 mM) conditions (Figure 3C) or knocking down Claudin-5 using siRNA (Figure 3D). The inhibition of the miR-200 and miR-466 by each of their inhibitor transfection was confirmed by real-time PCRs (Figures 3E and 3F). In the meantime, we used western blot analysis to detect Claudin-5 protein expressions in HDMECs upon high glucose treatment. Our results indicated that Claudin-5 protein levels were significantly reduced under high glucose conditions (Figure 3G). Furthermore, the inhibition of miR-466, but not miR-200, was able to restore Claudin-5 protein levels (Figure 3G). In this experiment, we also

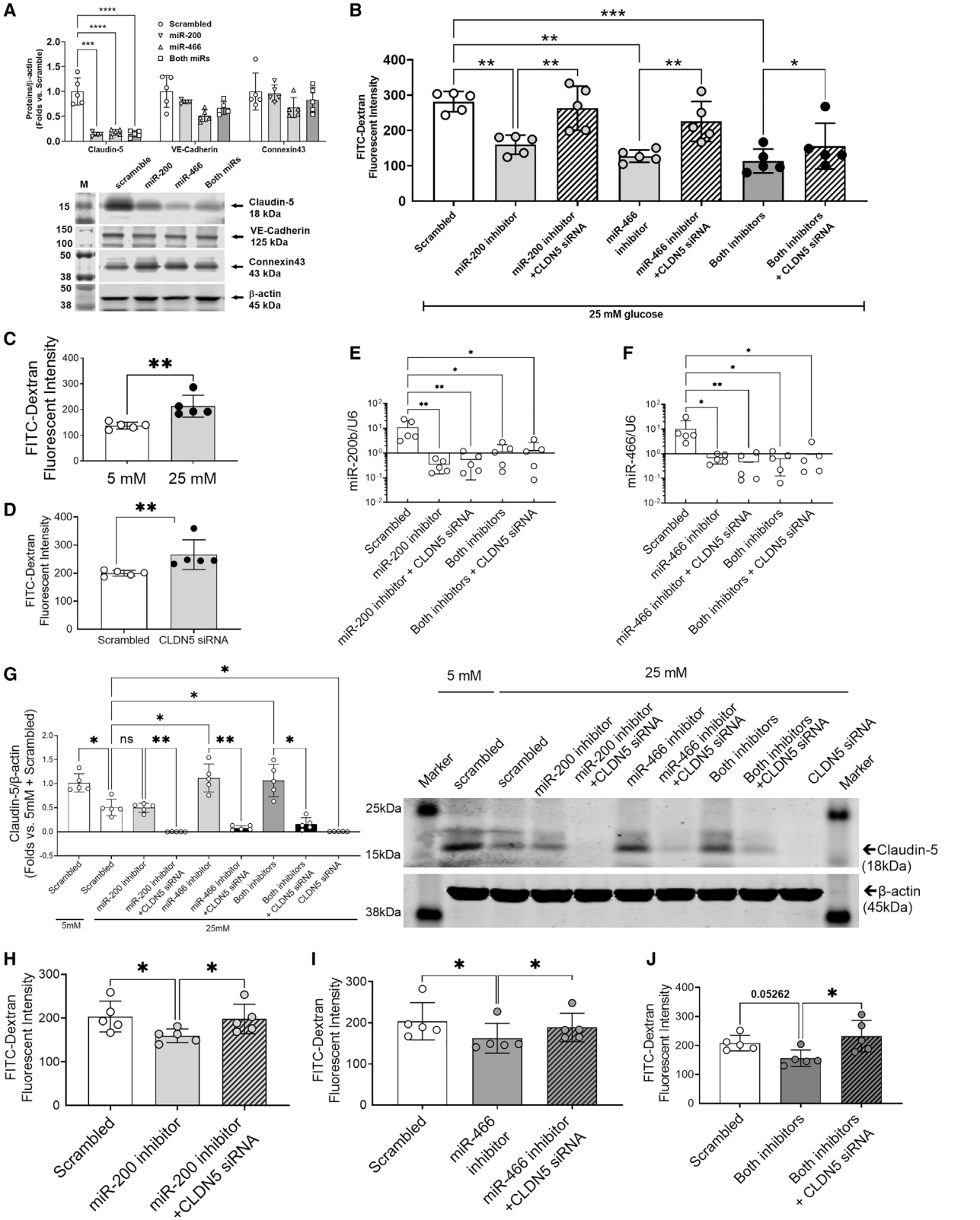


*(legend on next page)*

confirmed that the *CLDN5* siRNA knocked down Claudin-5 protein expressions by >90% (Figure 3G). Next, we examined the EC permeability in HDMECs transfected with either miR-200 inhibitor, miR-466 inhibitor, or both miR inhibitors, with or without simultaneous transfection of *CLDN5* siRNA. Our results demonstrated that the reduction of EC permeability by miR-200 inhibitor (Figure 3H) or miR-400 inhibitor (Figure 3I) was reversed by simultaneously knocking down Claudin-5. HDMECs treated with both miR-200 and miR-466 inhibitors (each at half-dose) demonstrated a trend of reducing EC permeability which was diminished by *CLDN5* siRNA (Figure 3J).

### Both miR-200 and miR-466 inhibit EC migration, but only miR-200 inhibits EC network formation *in vitro*

The angiogenic activities of ECs, including migration, network formation, and proliferation, were tested in healthy ECs with miR-200 and/or miR-466 overexpression. Our results suggested that both upregulation of miR-200 or miR-466 dampened EC migration (Figure 4A), but only miR-200 was able to suppress the network formation (Figure 4B). The cell proliferation was not affected by miR-200 or miR-466 (Figure 4C).

### Sequential application of miR-466 and/or miR-200 inhibitors rescue wound healing in animals with T2D

The efficacy of miR-200 and miR-466 were tested in a full-thickness excisional cutaneous wound model in animals with T2D. We tested the effectiveness of miR-466 inhibitor at 100 nM every other day in treating diabetic wounds. A moderate acceleration in wound closure was observed in the early inflammatory response phase. However, the overall time course of wound closure was comparable to that of the wounds receiving the control treatment (Figures 5A and 5B). In another set of experiments, we treated the diabetic wounds with a half-dose of miR-466 inhibitor (50 nM) and a half-dose of miR-200 inhibitor (50 nM) for the first 6 days only, then with a full dose of miR-200 inhibitor (100 nM) for the whole healing course (Figure 5C). Real-time PCRs suggested that the miR inhibitors had significantly inhibited the miR-200 and/or miR-466 levels in wound tissues (Figures 5D and 5E). The wound closure of the diabetic wounds receiving miR-200 inhibitor or control treatment was also recorded. Our results demonstrated that the miR-466 inhibitor on the first 6 days significantly enhanced the efficacy of the miR-200 inhibitor alone (Figures 5F and 5G). Furthermore, the histological analysis indicated no significant increase in capillary density formation induced by miR-466 inhibitor as suggested by CD31 staining (Figure 5H). MiR-200 inhibitor increased capillary density, and a short-term combination of miR-466 inhibitor amplified this effect. In fact, wounds receiving both miR-200 and miR-466 inhibitors demonstrated the highest capillary density among all of the groups (Figures 5H and 5I). In addition, the wound Claudin-5 levels were increased by either the miR-466 inhibitor alone or both the miR-200 + miR-466 inhibitors (Figures 5J and 5K). Despite this, the closure pace of miR-200- and miR-466-treated wounds in diabetic mice was slower than that of healthy mice (Figures 5F and 5G), suggesting that other defects hinder the wound healing in miR-200- and miR-466-treated wounds.

## DISCUSSION

This study aimed to investigate the roles of miR-200 and miR-466 in vascular permeability in diabetes. Our primary finding was that the upregulation of miR-200 and miR-466 resulted in the increase in EC permeability through targeting Claudin-5 under hyperglycemic conditions (Figure 6). In animals with hyperglycemia, the efficacy of miR-200 inhibitor on skin wound healing could be enhanced by co-administration of the miR-466 inhibitor at the early phase of injury. The study adds new knowledge for the synergistic regulation of miRs on vascular permeability and offers valuable data on the pre-clinical testing of miR cocktail therapies based on the dynamic needs for wound healing.

Different organisms can present various members of the miR family.[25] It is speculated that the genome positions of the miRs affect the capacity of the target gene or gene cluster silencing.[26] This is not the case for these two miRs. miR-200 and miR-466 are from different chromosomal locations in humans and mice and their mature sequences did not show similarity. However, reports have shown the simultaneous changes in miR-200 and miR-466 regardless of the model system. One typical example is that miR-200 and miR-466 are both sodium tonicity-response miRs.[15] To date, it is not clear how hyperglycemic conditions lead to the simultaneous upregulation of these two miRs. Our data indicated that not only osmotic pressure

**Figure 3. Inhibition of miR-200b or miR-466 decrease ECs permeability**

ECs from healthy donors were exposed to 25 mM glucose for 72 h together with miR inhibition, with or without Claudin-5 knockdown. (A) Protein expression of Claudin-5, VE-cadherin, and Connexin43 in healthy HAECs transfected with miR-200 or miR-466 precursors, compared to scrambled controls. n = 5 per group. Representative bands of western blot are shown below the quantification analysis. (B) FITC-dextran Transwell assay of healthy HAECs transfected with miR-200 inhibitor, or miR-400 inhibitor, or both miR inhibitors, with or without co-transfection of siRNA against *CLDN5*, after exposing them to 25 mM glucose for 72 h n = 5 per group. (C) FITC-dextran Transwell assay showing healthy HDMECs exposed to 25 mM glucose have higher permeability than control group exposed to 20 mM mannitol and 5 mM glucose. n = 5 per group. (D) FITC-dextran Transwell assay of permeability of HDMECs transfected with *CLDN5* siRNA or scrambled controls. n = 5 per group. (E) Real-time PCR of miR-200b levels in HDMECs transfected with miR-200 or miR-466 inhibitor, with or without co-transfection of *CLDN5* siRNA. (F) Real-time-PCR of miR-466 levels in HDMECs transfected with miR-200 or miR-466 inhibitor, with or without co-transfection of *CLDN5* siRNA. (G) Western blot assay showing the expression levels of Claudin-5 protein in HDMECs transfected with miR-200 or miR-466, or *CLDN5* siRNA after exposure to 25 mM glucose for 72 h, compared to scrambled control under 5 mM glucose and 20 mM mannitol. Representative bands of western blot are shown in the right panel. (H–J) FITC-dextran Transwell assay of healthy HDMECs transfected with miR-200 or miR-466 inhibitors, with or without co-transfection of *CLDN5* siRNA, using scrambled as controls. Data are presented as means ± SDs. *$p < 0.05$; **$p < 0.01$; ***$p < 0.001$; ****$p < 0.0001$; ns, not significant; M, marker. Mann-Whitney *U* test for statistical analysis (C and D); Kruskal-Wallis test and Mann-Whitney *U* test with Benjamini, Krieger, and Yekutieli's adjustment for multiple comparisons if significant (A and B and E–J).

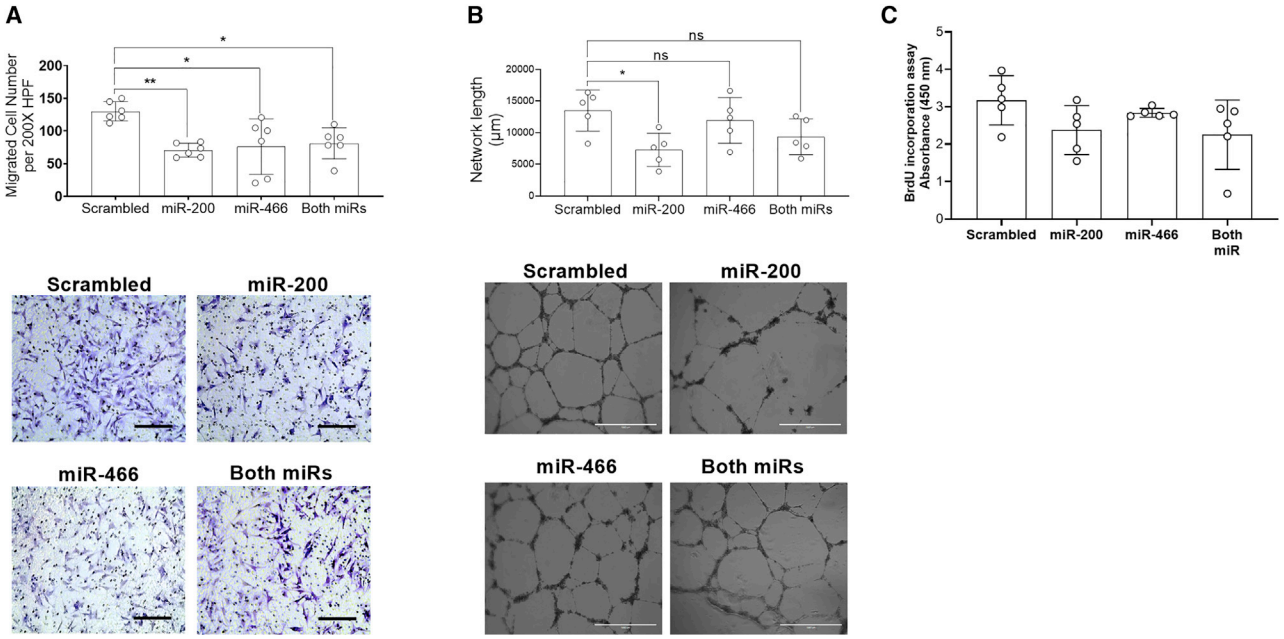


**Figure 4. Overexpression of miR-200 and miR-466 suppress ECs migration and network formation**

(A) Transwell migration assay of ECs transfected with miR-200 and/or miR-466, using scrambled as controls. Representative images are shown beneath the quantification analyses. Scale bar, 200 μm. n = 5 per group. (B) Network formation of ECs transfected with miR-200 and/or miR-466. Representative images are shown beneath the quantification analyses. Scale bar, 200 μm. n = 5 per group. (C) Bromodeoxyuridine (BrdU) proliferation assay of ECs transfected with miR-200 and/or miR-466. n = 5 per group. Data are presented as means ± SDs. *$p < 0.05$; **$p < 0.01$; ns, not significant. Kruskal-Wallis test and Mann-Whitney *U* test with Benjamini, Krieger, and Yekutieli's adjustment for multiple comparisons if significant.

but also high glucose per se induced miR-200 and miR-466 because the osmotic pressure was held comparable in high glucose (25 mM) and normal glucose (5 mM) treatments (Figure 1E). A recent genome-wide study observed a reduction in Dicer, an enzyme that produces mature miRs from precursor miRs, caused by sodium hyperosmotic challenge in gill filaments.[27] Similarly, we reported that Dicer transcript and protein levels were reduced in animal models of hyperglycemia.[24] In both scenarios, miR biogenesis should have been suppressed due to deficient Dicer processing. This could not explain the observations that many miRs, including miR-200 or miR-466, are upregulated. We have also shown that insufficient decay of precursor miRs by inositol requiring enzyme 1 in diabetes contributed to the upregulation of a subset of miRs, including miR-466 and miR-200 family members,[3] which could be a working mechanism for the upregulation of miR-200 and miR-466 in hyperglycemia to be tested in the future. Our study indicated that miR-466 overexpression decreased miR-200b/c levels, which added another layer of complexity in determining miR-miR interactions. Nonetheless, the connection between these two miR families remains elusive and warrants further investigations.

It is known that ECs of different vascular beds demonstrate phenotypic differences despite their similar angiogenic behaviors in response to vasoactive agents.[28,29] In our experiments, the macrovascular ECs (HAECs) from diabetic donors expressed higher levels of Claudin-5 (Figure 2A), while microvascular ECs (HDMECs) expressed modestly lower levels of Claudin-5 (Figure 2B). We are unsure whether this discrepancy was due to the different comorbidities of the diabetic donors since there was only limited disease information available. However, in HAECs and HDMECs, miR-200 and miR-466 both inhibit Claudin-5 protein expression and increase EC permeability. Microvascular ECs may rely more on Claudin-5, compared to the other ECs,[30] as knockdown of Claudin-5 in HDMECs causes a significant increase in permeability (Figure 3D). The miR-466 inhibition is more potent in rescuing Claudin-5 and reducing EC permeability than miR-200 (Figures 3G–3I). It is likely that miR-466 inhibition reduces EC permeability through multiple direct or indirect mechanisms, an interesting question to be elucidated for future investigation.

Wound healing involves a finely orchestrated, self-limiting series of cellular and molecular events, resulting in transient increases in vascular permeability and angiogenesis.[31] Increased vascular permeability is a natural consequence of inflammation upon wounding and allows more cytokine extravasation and leukocyte recruitment.[32] The tissue injury and the cytokine extravasation also induce a vigorous angiogenesis response—that is, the growth of leaky capillaries from the existing vasculature.[33] Despite their highly permeable nature, these newly formed vessels help support granulation tissue formation and re-epithelialization, which rebuild the dermis structure. However, excessive and prolonged vascular permeability creates an edemic and inflammatory environment, disturbing the transition

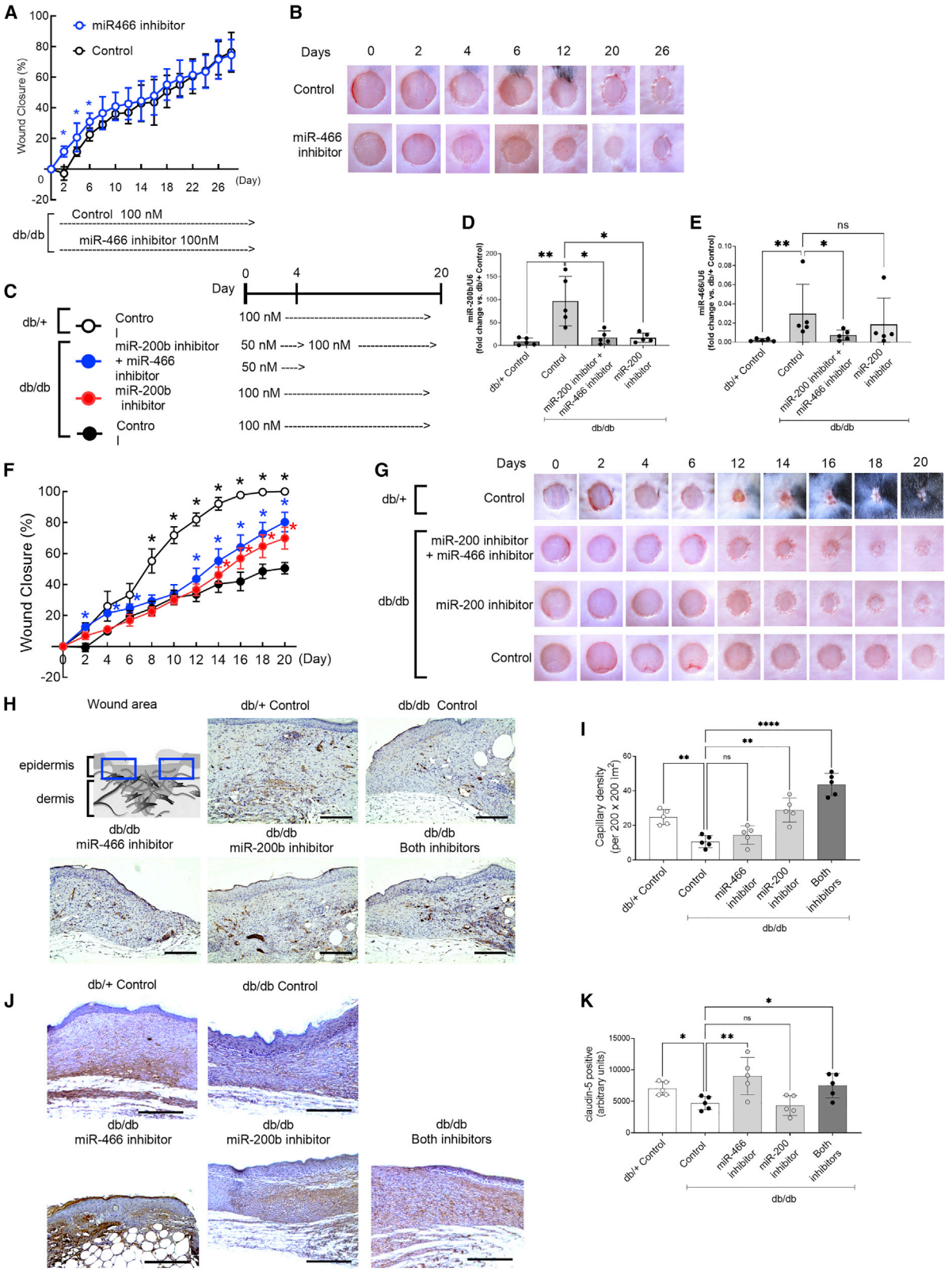


*(legend on next page)*

of wound tissue from the proliferative phase to the remodeling phase.[34] Our *in vitro* data indicated that miR-200 overexpression augmented EC network formation and migration (Figures 4A and 4B). In contrast, miR-466 overexpression suppressed EC migration but did not inhibit EC network formation, suggesting that miR-200 is more potent in inhibiting angiogenesis than miR-466. However, miR-466 is more potent in increasing EC permeability than miR-200 (Figure 1G). Simultaneous treatment of both miRs did not increase EC permeability any further (Figure 1G). This is important because timely and self-limiting control over vascular permeability is critical for wound healing. MiR-200 inhibition has been shown to increase the expression of vascular endothelial growth factor/receptor 2 (VEGF/VEGFR2), which promotes local angiogenesis. However, the randomized clinical trials using VEGF as a proangiogenic agent to treat diabetic wounds have not lived up to expectations, and clinical efficacy remains uncertain.[35] Increased tissue edema due to vascular hyperpermeability seems to be one of the contributing factors to the compromised effectiveness. In the present study, we tested whether controlling vascular permeability by adding miRs that control EC permeability could improve the efficacy. In the early phase of normal wound healing, there is a transient decrease in miR-200 levels in keratinocytes and dermal wound-edge ECs, allowing cell proliferation and migration to occur.[22,23] However, in diabetes, the downregulation of miR-200 was absent. MiR-200 has been proposed as an excellent target in diabetic wounds, due to not only its proinflammatory and anti-angiogenic actions[36] but also its role in compromising keratinocyte and fibroblast functions.[23,37] The topical delivery of the miR inhibitors to the wound bed affects not only ECs but also several other cell types in the skin, including keratinocytes and fibroblasts. The efficacy of miR inhibitors on accelerating wound closure is likely associated with the combined efforts of the inhibitors on all of the cell types involved in the wounds.

miR-466 has been recognized as a potent suppressor of oncogenes,[38] inhibiting cell proliferation through several molecules.[39,40] We anticipated that miR-466 inhibitor would show similar efficacy as miR-200 inhibitor. However, the application of miR-466 inhibitor only showed improvement in wound closure during the first 6 days (Figure 5A). We speculated that the constant increase in vascular permeability was not helpful in the proliferative or remodeling phases. In the meantime, miR-200 inhibitor-treated wounds showed an acceleration of wound healing starting from day 14 compared to wounds with the control treatment. The temporary use of miR-466 inhibitor (days 0, 2, 4) enhanced the efficacy of miR-200 inhibitor (Figures 5F and 5G), with the acceleration of wound closure at the beginning (days 2–6) and then in the remodeling phase of wound healing (days 12–20), compared with the control treatment. Furthermore, the miR-200 and miR-466 inhibitor-treated wounds were covered by a slightly keratinized epithelial layer as early as day 16, while other treatment groups had open wet wounds. The number of oligonucleotides loaded onto the wound bed was comparable among all of the treatment groups. Admittedly, the dosing of oligonucleotides needs to be optimized because the wounds receiving miR inhibitors did not heal as fast as the wounds in healthy mice. One more factor to consider was that both miR-200 and miR-466 were reduced to half-dose when they were used together to treat the cells or the wounds, compared with the single miR inhibitor treatment. This may have contributed to the lesser extent of changes in cell permeability or wound healing when compared with the single inhibitor group. It is challenging for us to evaluate this functional outcome because vascular permeability is usually measured in the skin with an intact epidermis. For example, the Miles assay is used to detect the skin accumulation of the intravenously administered tracers (e.g., Evans blue) that bind to albumin after the local administration of stimulants.[33] Another method is the detection of intravenously administrated fluorescein-conjugated dextrans (<70 kDa) using two-photon microscopy attached to the skin.[41] Because our wound surgery created a defect in the dermis and epidermis, it is inaccurate to measure the outcome of the methods mentioned above. However, it would be of great interest in our future studies. Another technique that may limit the efficacy was that the oligonucleotide-transferring mixture was administered through topical dispensation onto the wound bed instead of multi-point injections at wound edges to create minimal perturbation of tissue regeneration. Despite these limitations, the outcome of the animal study suggests a potentially promising approach to using miR cocktail therapies in wound healing.

In summary, our study indicated that the elevation of miR-466 and miR-200 in diabetes damaged EC integrity and increased cell permeability by targeting Claudin-5. This contributed to the tissue edema in

**Figure 5. miR-466 and/or miR-200 inhibitors accelerated wound healing in T2D mice**

A mouse model of leptin receptor-deficient mice (BKS.Cg-m$^{+/+}$ Lepr$^{db}$/J, db/db) and their healthy littermates (BKS.Cg-m$^{-/-}$ Lep$^{db/-}$ lean, db/+) was used. A full-thickness standard-size excisional wound was created on the dorsal skin. (A) Wound closure curves in db/db mice that received topical delivery of 100 nM miR-466 inhibitor or scramble controls onto the excisional wound. n = 4–5 per group. (B) Representative images of cutaneous wounds taken on days 0, 2, 4, 6, 12, 20, and 26 after wounding. (C) The dosage and time of the administration of miR-466 and/or miR-200 inhibitor, or scramble control on db/db or db/+ mice. (D and E) Real-time-PCR of miR-200 and miR-466 levels in wound tissues isolated from the mice received administration of miR-466 or miR-200 inhibitors, or scramble control onto the wounds. (F) Wound closure curves in db/db or db/+ mice which received topical delivery of miR-466 and/or miR-200 inhibitor, or scramble control onto the excisional wound. (G) Representative images of cutaneous wounds taken on days 0, 2, 4, 6, 12, 14, 16, 18, and 20 after wounding. (H) Representative images of CD31 staining of the wound bed isolated from db/db or db/+ mice that received miR-200 and/or miR-466 inhibitor, or scramble controls. Scale bar, 200 μm. (I) Capillary density on wound samples from db/db or db/+ mice that received miR-200 and/or miR-466 inhibitor, or scramble controls. (J) Immunohistochemistry staining of Claudin-5 protein on wound samples from db/db or db/+ mice that received miR-200 and/or miR-466 inhibitor or scramble controls. Scale bar, 200 μm. (K) Claudin-5$^{+}$ area on wound samples from db/db or db/+ mice that received miR-200 and/or miR-466 inhibitor, or scramble controls. Data are presented as means ± SDs. *$p < 0.05$; **$p < 0.01$; ****$p < 0.0001$; ns, not significant. The statistical analysis used for each bar graph: Mann-Whitney *U* test for (A); Kruskal-Wallis test and Mann-Whitney *U* test with Benjamini, Krieger, and Yekutieli's adjustment for multiple comparisons if significant for (D)–(F), (I), and (K).

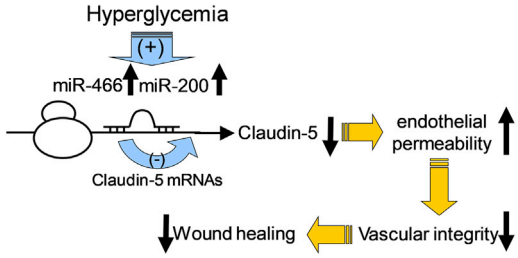


**Figure 6. miR-200 and miR466 regulation of vascular permeability and their predominant mode of action**

Under hyperglycemic conditions, miR-466 and miR-200 were upregulated in ECs. These 2 miR families repress Claudin-5 mRNA translation, leading to a decrease in Claudin-5 proteins. As a result, the downregulated Claudin-5 by increased miR-466 and miR-200 activities contributes to increased vascular permeability, decreased angiogenesis, and ineffective wound tissue repair in diabetes.

the early phase of wound healing, which disturbed the healing process. The miR-200/466 system may offer a therapeutic approach for orchestrating vascular permeability homeostasis in normal physiological diseases. Antisense-based therapeutic targeting of miRs such as miR-200/466 may serve as a novel avenue for the treatment of vaso-pathological disorders associated with metabolic syndrome.

## MATERIALS AND METHODS

### HAEC culture and HDMEC culture

HAECs from healthy donors and patients with T2D were purchased from Lonza (Basel, Switzerland) and maintained in EGM-2 (Lonza) plus 5% fetal bovine serum in 37°C, 5% $CO_2$.[42] Donor information: healthy donors, n = 5, age 54.270 ± 3.03 years, male:female = 3:2; T2D donors, n = 5, age 60.60 ± 6.31 years, male:female = 3:2. Both healthy ECs and diabetic HAECs underwent 4–7 passage cycles and were grown until they were 70%–90% confluent.[43] HDMECs from healthy donors and patients with T2D were purchased from Lonza and maintained in microvascular EGM-2 (EGM-2 MV, Lonza) in 37°C, 5% $CO_2$. Donor information: healthy donors, n = 5, age 58.8 ± 1.068 years, male:female = 1:4; T2D donors, n = 3, age 60.67 ± 2.028 years, male:female = 2:1. All of the HDMECs underwent 4–7 passage cycles and were grown until they were 70%–90% confluent.

### Real-time PCR analysis

The miRs were extracted using the miRNAeasy Kit (Qiagen, Germantown, MD, USA). The cDNA was synthesized using miRCURY LNA RT Kit (Qiagen). A real-time PCR was performed to determine levels of miR-466 and miR-200 family members, including miR-200a/b/c, miR-141, and miR249, using U6 as the internal control (primer sets from Qiagen). The initial threshold determined cycle threshold (Ct) values, and the relative expression of RNA was calculated by the comparative ΔΔCt method.

### Endothelial permeability assay

Endothelial permeability was tested as previously described.[44] ECs were grown to confluence for a minimum of 3 days in the top well of a Transwell filter (0.4 μm, 12-mm diameter, Corning, Corning, NY, USA). Treatment doses and times are as detailed in the figure legends. The isothiocyanate-dextran FITC-labeled fluorescent dye (FITC-Dextran, average 10,000 molecular weight, Thermo Fisher Scientific, Waltham, MA, USA) was added to the top chamber of the Transwell for a final concentration of 1 mg/mL. Permeability was measured by detecting the fluorescent intensity of the amount of dye that leaked through the Transwell filter and reached the lower chamber within 2 h. The fluorescence signal was recorded using GloMax Explorer fluorescent reader (excitation 475 nm, emission 495–505).[44]

### miR manipulations

The ECs grown to 70%–90% confluence were transfected with 5 nM miR-200b stem-loop precursor (PM10492, stem-loop accession number: miRBase: MI0000342), or 5 nM miR-466 stem-loop precursor (PM18443, stem-loop accession number: miRBase: MI0014157), or 5 nM Pre-miR miRNA Precursor Negative Control (AM17110, all purchased from Thermo Fisher Scientific) by using Lipofectamine RNAiMAX Reagent (Invitrogen, Waltham, MA, USA) according to the manufacturer's instructions. For the inhibition of miRs, ECs were transfected with miR-200b inhibitor (AM10492, stem-loop accession number: miRBase: MIMAT0000318), or miR466 inhibitor (AM18443, stem-loop accession number: miRBase: MI0014157), or Anti-miR miRNA Inhibitor Negative Control #1 (AM17010, all from Thermo Fisher Scientific) by using Lipofectamine RNAiMAX Reagent. Cells were incubated at 37°C for 48–72 h before being harvested for experiments.

### Cell functional tests, including migration, proliferation, and network formation

The ECs were subcultured into the upper chamber of a 24-well Transwell plate at a density of $3 \times 10^4$ cells/well in serum-free EGM-2 media. An amount of 600 μL EGM-2 with 10% fetal bovine serum was added to the lower chamber. The cells were then incubated for 16 h. Media in the upper and lower chambers were discarded, and the inserts were washed with PBS twice. The cells remaining in the upper chamber were gently removed by scraping with a cotton sponge and then were rinsed with PBS twice. The ECs were fixed with 10% formalin for 10 min and stained with 0.5% crystal violet for 30 min at room temperature. The insert membrane was then washed with PBS six times until transparent. Images were taken using EVOS FL Imaging System (Thermo Fisher Scientific). The number of cells that migrated to the lower side of the membrane was counted and recorded as the migrated cells per 200× high-power field.

### Western blot analysis

Cells were lysed using Cell Lytic MT lysis buffer (Sigma-Aldrich, St. Louis, MO, USA) with Protease Inhibitor Cocktail (1:100 v/v, Thermo Fisher Scientific) for 20 min on ice. The lysate was sonicated at 20% amplitude for 30 s on ice. The protein concentration was determined by Bradford assay using Quick Start™ Bradford 1 X Dye Reagent (Bio-Rad, Hercules, CA, USA). Equal amounts of denatured protein (30 μg) were separated by SDS-PAGE on 10% Tris-glycine

polyacrylamide gels and transferred to a 0.45-μm polyvinylidene fluoride membrane (Sigma-Aldrich) together with Chameleon Duo Prestained Protein Ladder (Li-Cor, Lincoln, NE, USA). Immunoblotting was performed by using antibodies directed against each target molecule: Claudin-5 (1:1,000, Invitrogen), Connexin43 (1:1,000, Abcam, Cambridge, UK), and VE-cadherin (1:1,000, R&D, Minneapolis, MN, USA). The housekeeping protein was β-actin (1:10,000, Cell Signaling Technology, Danvers, MA, USA). Secondary antibodies, including IRDye donkey anti-goat IgG (1:20,000), IRdye goat anti-mouse IgG (1:20,000), and IRdye goat anti-rabbit IgG (1:20,000) from Li-Cor were incubated at room temperature for 1 h. For the immunoblotting of two target proteins with close molecular weight on the same membrane, such as Connexin43 and β-actin, we did not strip the membrane between two probings as the secondary antibodies for Connexin43 and β-actin are from different species and are conjugated with different fluorescent dyes. These two secondary antibodies ensure minimum or no signal interference between separate channels in the fluorescent imaging system. Membrane-bound antibody fluorescence signals were detected by Li-Cor Odyssey CLx. Quantitative analysis of protein levels was analyzed with Image Studio Lite version 5.2 (Li-Cor). The target protein expression was divided by β-actin to get the relative abundance (considered as the first delta) in each sample. The mean value of the control group was calculated, and the value of each sample was then divided by the mean value to obtain the fold change (considered as the second delta). The data were presented as the fold change versus the control treatment group.

#### 3′ UTR luciferase activity assays

Synthetic oligonucleotides of human *Claudin-5* (*CLDN5*) mRNA 3′ UTR (Target Gene Accession: NM_003,277.3) were cloned into a luciferase reporter vector system (SwitchGear, Carlsbad, CA, USA). Healthy ECs were co-transfected with 100 ng *CLDN5* 3′ UTR reporter and 0.1 nmol miR precursors, either miR-200 or miR-466, or 0.1 nmol scramble controls (all purchased from Ambion, Waltham, MA, USA) using DharmaFECT Duo transfection reagent (Dharmacon, Lafayette, CO, USA) according to the manufacturer's protocol. After 48 h, luciferase activity was measured. A reduced firefly luciferase expression indicates the direct binding of miRs to the cloned target sequence.

#### Cutaneous wound healing with miR-200 and miR-466 inhibitors in diabetic animals

Male T2D mice (BKS.Cg-m$^{+/+}$ Lepr$^{db}$/J, db/db, age 12–14 weeks, blood glucose over 250 mg/dL) and their age- and sex-matched nondiabetic healthy littermates (BKS.Cg-m$^{-/-}$ Lep$^{db/-}$ lean, db/+, blood glucose 123.80 ± 19.72 mg/dL) were purchased from the Jackson Laboratory (Bar Harbor, ME, USA). A full-thickness excisional wound was created on dorsal skin using a 7-mm punch biopsy without damaging the underlying muscles, as we previously described.[3,24,45] For topical delivery of miR inhibitors, anti-miR miRNA inhibitor (Thermo Fisher Scientific), 100 nM miRNA inhibitor in Lipofectamine™ RNAiMAX (Invitrogen) in 50 μL of Opti-MEM were topically placed onto the wound bed immediately after punch. The grouping was as follows: (1) db/db wound with 100 nM scrambled control (anti-miR negative control #1, Ambion); (2) db/db wound with 100 nM miR-200b inhibitor (50 nM hsa-miR-200-5p and 50 nM hsa-miR-200-3p, Ambion); (3) db/db wound with 50 nM miR-466a inhibitor (25 nM mmu-miR-466-5p and 25 nM mmu-miR-466-3p, Ambion) and 50 nM of miR-200b inhibitor on days 0, 2, and 4, followed by 100 nM miR-200b inhibitor for the remaining days; and (4) db/+ wound with 100 nM scramble control. Immediately after, wounds were covered with a transparent oxygen-permeable wound dressing (Tegaderm™ film, 3M Medical, Eden Prairie, MN, USA). A freshly prepared miRNA inhibitor was administrated on the wound every other day with the change of dressing. Wound closure rates were calculated as percentage closed (y%) = [(area on day$_0$ – open area on day$_x$)/area on day$_0$] × 100. On day 20 after wounding, wounds and the adjacent skin were collected for CD31 and Claudin-5 immunochemistry staining. All of the animal procedures were performed according to Wayne State University Institutional Animal Care and Use Committee (IACUC) guidelines.

#### Statistical analyses

All of the values are expressed as means ± SDs. For continuous variables that failed Shapiro-Wilk normality tests such as miR expression, protein levels, staining quantifications, and functional assays, the statistical significance of differences between the two groups was determined by the Mann-Whitney *U* test. When more than two groups of treatments were performed, we used the Kruskal-Wallis test across all of the groups. If significant, we then tested the pairs of our primary interest based on scientific rationale using the Mann-Whitney *U* test with Benjamini, Krieger, and Yekutieli's adjustment for multiple comparisons.[46] Due to multiple hypothesis testing, these gatekeeping approaches and the adjustments can preserve the alpha spending and control false positive rate inflation (<0.05). The significant differences that came from post hoc comparisons of groups were noted. A value of $p < 0.05$ was considered statistically significant. All of the statistical analyses were performed using GraphPad Prism 9 (GraphPad Software, San Diego, CA, USA).

## DATA AVAILABILITY STATEMENT

The dataset generated in this study are available from the corresponding author upon reasonable request.

## ACKNOWLEDGMENTS

This work was supported in part by NIH/NIDDK R01 DK109036, R01 DK119222, and R01 DK128937 (to J.-M.W.). M.M. was supported by the institutional training grant IMSD at Wayne State University (T32 GM 139807). We thank the Department of Laboratory Animal Research staff at Wayne State University for providing excellent animal care.

## AUTHOR CONTRIBUTIONS

M.K. and M.O. conducted the *in vitro* experiments, collected and analyzed the data, and wrote the manuscript; H.L. conducted the *in vitro* experiments and the *in vivo* wound healing experiments and edited the manuscript; L.X. assisted with the experiments for

western blot and data acquisition; S.P.M.V., H.N., M.M., and K.Z. contributed to data interpretation and edited the manuscript. J.-M.W. designed the experiments, performed data analysis and interpretation, and wrote the manuscript.

## DECLARATION OF INTERESTS

The authors declare no competing interests.

## REFERENCES


1. Takeo, M., Lee, W., and Ito, M. (2015). Wound healing and skin regeneration. Cold Spring Harb. Perspect. Med. *5*, a023267. https://doi.org/10.1101/cshperspect.a023267.
2. Cañedo-Dorantes, L., and Cañedo-Ayala, M. (2019). Skin acute wound healing: a comprehensive review. Int. J. Inflam. *2019*, 3706315. https://doi.org/10.1155/2019/3706315.
3. Wang, J.M., Qiu, Y., Yang, Z.Q., Li, L., and Zhang, K. (2017). Inositol-requiring enzyme 1 facilitates diabetic wound healing through modulating MicroRNAs. Diabetes *66*, 177–192. https://doi.org/10.2337/db16-0052.
4. Armstrong, D.G., Boulton, A.J.M., and Bus, S.A. (2017). Diabetic foot ulcers and their recurrence. N. Engl. J. Med. *376*, 2367–2375. https://doi.org/10.1056/NEJMra1615439.
5. Rodrigues, M., Kosaric, N., Bonham, C.A., and Gurtner, G.C. (2019). Wound healing: a cellular perspective. Physiol. Rev. *99*, 665–706. https://doi.org/10.1152/physrev.00067.2017.
6. Okonkwo, U.A., Chen, L., Ma, D., Haywood, V.A., Barakat, M., Urao, N., and DiPietro, L.A. (2020). Compromised angiogenesis and vascular Integrity in impaired diabetic wound healing. PLoS One *15*, e0231962. https://doi.org/10.1371/journal.pone.0231962.
7. Zhang, H.N., Xu, Q.Q., Thakur, A., Alfred, M.O., Chakraborty, M., Ghosh, A., and Yu, X.B. (2018). Endothelial dysfunction in diabetes and hypertension: role of microRNAs and long non-coding RNAs. Life Sci. *213*, 258–268. https://doi.org/10.1016/j.lfs.2018.10.028.
8. Mundi, S., Massaro, M., Scoditti, E., Carluccio, M.A., van Hinsbergh, V.W.M., Iruela-Arispe, M.L., and De Caterina, R. (2018). Endothelial permeability, LDL deposition, and cardiovascular risk factors-a review. Cardiovasc. Res. *114*, 35–52. https://doi.org/10.1093/cvr/cvx226.
9. Schneeberger, E.E., and Lynch, R.D. (2004). The tight junction: a multifunctional complex. Am. J. Physiol. Cell Physiol. *286*, C1213–C1228. https://doi.org/10.1152/ajpcell.00558.2003.
10. Vermette, D., Hu, P., Canarie, M.F., Funaro, M., Glover, J., and Pierce, R.W. (2018). Tight junction structure, function, and assessment in the critically ill: a systematic review. Intensive Care Med. Exp. *6*, 37. https://doi.org/10.1186/s40635-018-0203-4.
11. Nitta, T., Hata, M., Gotoh, S., Seo, Y., Sasaki, H., Hashimoto, N., Furuse, M., and Tsukita, S. (2003). Size-selective loosening of the blood-brain barrier in claudin-5-deficient mice. J. Cell Biol. *161*, 653–660. https://doi.org/10.1083/jcb.200302070.
12. Nagai, M.K., and Embil, J.M. (2002). Becaplermin: recombinant platelet derived growth factor, a new treatment for healing diabetic foot ulcers. Expert Opin. Biol. Ther. *2*, 211–218. https://doi.org/10.1517/14712598.2.2.211.
13. Cao, Y., Gang, X., Sun, C., and Wang, G. (2017). Mesenchymal stem cells improve healing of diabetic foot ulcer. J. Diabetes Res. *2017*, 9328347. https://doi.org/10.1155/2017/9328347.
14. Krol, J., Loedige, I., and Filipowicz, W. (2010). The widespread regulation of microRNA biogenesis, function and decay. Nat. Rev. Genet. *11*, 597–610. https://doi.org/10.1038/nrg2843.
15. Luo, Y., Liu, Y., Liu, M., Wei, J., Zhang, Y., Hou, J., Huang, W., Wang, T., Li, X., He, Y., et al. (2014). Sfmbt2 10th intron-hosted miR-466(a/e)-3p are important epigenetic regulators of Nfat5 signaling, osmoregulation and urine concentration in mice. Biochim. Biophys. Acta *1839*, 97–106. https://doi.org/10.1016/j.bbagrm.2013.12.005.
16. Liamis, G., Liberopoulos, E., Barkas, F., and Elisaf, M. (2014). Diabetes mellitus and electrolyte disorders. World J. Clin. Cases *2*, 488–496. https://doi.org/10.12998/wjcc.v2.i10.488.
17. Soreq, H. (2014). Novel roles of non-coding brain RNAs in health and disease. Front. Mol. Neurosci. *7*, 55. https://doi.org/10.3389/fnmol.2014.00055.
18. Katsuyama, E., Yan, M., Watanabe, K.S., Narazaki, M., Matsushima, S., Yamamura, Y., Hiramatsu, S., Ohashi, K., Watanabe, H., Katsuyama, T., et al. (2017). Downregulation of miR-200a-3p, targeting CtBP2 complex, is involved in the hyperproduction of IL-2 in systemic lupus erythematosus-derived T cells. J. Immunol. *198*, 4268–4276. https://doi.org/10.4049/jimmunol.1601705.
19. Aunin, E., Broadley, D., Ahmed, M.I., Mardaryev, A.N., and Botchkareva, N.V. (2017). Exploring a role for regulatory miRNAs in wound healing during ageing:involvement of miR-200c in wound repair. Sci. Rep. *7*, 3257. https://doi.org/10.1038/s41598-017-03331-6.
20. Humphries, B., and Yang, C. (2015). The microRNA-200 family: small molecules with novel roles in cancer development, progression and therapy. Oncotarget *6*, 6472–6498. https://doi.org/10.18632/oncotarget.3052.
21. Zhang, H., Liu, J., Qu, D., Wang, L., Luo, J.Y., Lau, C.W., Liu, P., Gao, Z., Tipoe, G.L., Lee, H.K., et al. (2016). Inhibition of miR-200c restores endothelial function in diabetic mice through suppression of COX-2. Diabetes *65*, 1196–1207. https://doi.org/10.2337/db15-1067.
22. Chan, Y.C., Roy, S., Khanna, S., and Sen, C.K. (2012). Downregulation of endothelial microRNA-200b supports cutaneous wound angiogenesis by desilencing GATA binding protein 2 and vascular endothelial growth factor receptor 2. Arterioscler. Thromb. Vasc. Biol. *32*, 1372–1382. https://doi.org/10.1161/ATVBAHA.112.248583.
23. Tang, H., Wang, X., Zhang, M., Yan, Y., Huang, S., Ji, J., Xu, J., Zhang, Y., Cai, Y., Yang, B., et al. (2020). MicroRNA-200b/c-3p regulate epithelial plasticity and inhibit cutaneous wound healing by modulating TGF-beta-mediated RAC1 signaling. Cell Death Dis. *11*, 931. https://doi.org/10.1038/s41419-020-03132-2.
24. Wang, J.M., Tao, J., Chen, D.D., Cai, J.J., Irani, K., Wang, Q., Yuan, H., and Chen, A.F. (2014). MicroRNA miR-27b rescues bone marrow-derived angiogenic cell function and accelerates wound healing in type 2 diabetes mellitus. Arterioscler. Thromb. Vasc. Biol. *34*, 99–109. https://doi.org/10.1161/ATVBAHA.113.302104.
25. Pal, A.S., and Kasinski, A.L. (2017). Animal models to study MicroRNA function. Adv. Cancer Res. *135*, 53–118. https://doi.org/10.1016/bs.acr.2017.06.006.
26. Calin, G.A., Sevignani, C., Dumitru, C.D., Hyslop, T., Noch, E., Yendamuri, S., Shimizu, M., Rattan, S., Bullrich, F., Negrini, M., and Croce, C.M. (2004). Human microRNA genes are frequently located at fragile sites and genomic regions involved in cancers. Proc. Natl. Acad. Sci. USA *101*, 2999–3004. https://doi.org/10.1073/pnas.0307323101.
27. Ng, H.M., Ho, J.C.H., Nong, W., Hui, J.H.L., Lai, K.P., and Wong, C.K.C. (2020). Genome-wide analysis of MicroRNA-messenger RNA interactome in ex-vivo gill filaments, Anguilla japonica. BMC Genom. *21*, 208. https://doi.org/10.1186/s12864-020-6630-0.
28. Aird, W.C. (2007). Phenotypic heterogeneity of the endothelium: II. Representative vascular beds. Circ. Res. *100*, 174–190. https://doi.org/10.1161/01.RES.0000255690.03436.
29. Aird, W.C. (2007). Phenotypic heterogeneity of the endothelium: I. Structure, function, and mechanisms. Circ. Res. *100*, 158–173. https://doi.org/10.1161/01.RES.0000255691.76142.4a.
30. Kluger, M.S., Clark, P.R., Tellides, G., Gerke, V., and Pober, J.S. (2013). Claudin-5 controls intercellular barriers of human dermal microvascular but not human umbilical vein endothelial cells. Arterioscler. Thromb. Vasc. Biol. *33*, 489–500. https://doi.org/10.1161/ATVBAHA.112.300893.
31. Demidova-Rice, T.N., Hamblin, M.R., and Herman, I.M. (2012). Acute and impaired wound healing: pathophysiology and current methods for drug delivery, part 2: role of growth factors in normal and pathological wound healing: therapeutic potential and methods of delivery. Adv. Skin Wound Care *25*, 349–370. https://doi.org/10.1097/01.ASW.0000418541.31366.a3.
32. Laviv, Y., Kasper, B., and Kasper, E.M. (2018). Vascular hyperpermeability as a hallmark of phacomatoses: is the etiology angiogenesis related to or comparable with mechanisms seen in inflammatory pathways? Part II: angiogenesis- and inflammation-related molecular pathways, tumor-associated macrophages, and possible therapeutic implications: a comprehensive review. Neurosurg. Rev. *41*, 931–944. https://doi.org/10.1007/s10143-017-0837-9.

33. Nagy, J.A., Benjamin, L., Zeng, H., Dvorak, A.M., and Dvorak, H.F. (2008). Vascular permeability, vascular hyperpermeability and angiogenesis. Angiogenesis *11*, 109–119. https://doi.org/10.1007/s10456-008-9099-z.

34. Mittal, M., Siddiqui, M.R., Tran, K., Reddy, S.P., and Malik, A.B. (2014). Reactive oxygen species in inflammation and tissue injury. Antioxid. Redox Signal. *20*, 1126–1167. https://doi.org/10.1089/ars.2012.5149.

35. Giacca, M., and Zacchigna, S. (2012). VEGF gene therapy: therapeutic angiogenesis in the clinic and beyond. Gene Ther. *19*, 622–629. https://doi.org/10.1038/gt.2012.17.

36. Lo, W.Y., Yang, W.K., Peng, C.T., Pai, W.Y., and Wang, H.J. (2018). MicroRNA-200a/200b modulate high glucose-induced endothelial inflammation by targeting O-linked N-acetylglucosamine transferase expression. Front. Physiol. *9*, 355. https://doi.org/10.3389/fphys.2018.00355.

37. Zhou, R., Wang, C., Liang, Y., Li, X., and Li, Q. (2019). Anti-miR-200b promotes wound healing by regulating fibroblast functions in a novel mouse model. Acta Biochim. Biophys. Sin. *51*, 1049–1055. https://doi.org/10.1093/abbs/gmz091.

38. Colden, M., Dar, A.A., Saini, S., Dahiya, P.V., Shahryari, V., Yamamura, S., Tanaka, Y., Stein, G., Dahiya, R., and Majid, S. (2017). MicroRNA-466 inhibits tumor growth and bone metastasis in prostate cancer by direct regulation of osteogenic transcription factor RUNX2. Cell Death Dis. *8*, e2572. https://doi.org/10.1038/cddis.2017.15.

39. Haig, D., and Mainieri, A. (2020). The evolution of imprinted microRNAs and their RNA targets. Genes *11*, E1038. https://doi.org/10.3390/genes11091038.

40. Malnou, E.C., Umlauf, D., Mouysset, M., and Cavaillé, J. (2018). Imprinted MicroRNA gene clusters in the evolution, development, and functions of mammalian placenta. Front. Genet. *9*, 706. https://doi.org/10.3389/fgene.2018.00706.

41. Ono, S., Egawa, G., and Kabashima, K. (2017). Regulation of blood vascular permeability in the skin. Inflamm. Regen. *37*, 11. https://doi.org/10.1186/s41232-017-0042-9.

42. Jiang, R., Cai, J., Zhu, Z., Chen, D., Wang, J., Wang, Q., Teng, Y., Huang, Y., Tao, M., Xia, A., et al. (2014). Hypoxic trophoblast HMGB1 induces endothelial cell hyperpermeability via the TRL-4/caveolin-1 pathway. J. Immunol. *193*, 5000–5012. https://doi.org/10.4049/jimmunol.1303445.

43. Zhou, L., Zhang, H.H., Chen, N., Zhang, Z.B., Liu, M., Dai, L.F., Wang, J.M., Jiang, Y.W., and Wu, Y. (2019). Clinical features of 54 cases of leukoencephalopathy with vanishing white matter disease in children. Zhonghua Er Ke Za Zhi *57*, 837–843. https://doi.org/10.3760/cma.j.issn.0578-1310.2019.11.005.

44. Monaghan-Benson, E., and Burridge, K. (2009). The regulation of vascular endothelial growth factor-induced microvascular permeability requires Rac and reactive oxygen species. J. Biol. Chem. *284*, 25602–25611. https://doi.org/10.1074/jbc.M109.009894.

45. Lang, J., Xu, F.J., Ge, W.K., Liu, B.Y., Zhang, N., Sun, Y.H., Wang, J.M., Wang, M.X., Xie, N., Fang, X.Z., et al. (2019). Greatly enhanced performance of AlGaN-based deep ultraviolet light emitting diodes by introducing a polarization modulated electron blocking layer. Opt Express *27*, A1458–A1466. https://doi.org/10.1364/OE.27.0A1458.

46. Benjamini, Y., Krieger, A.M., and Yekutieli, D. (2006). Adaptive linear step-up procedures that control the false discovery rate. Biometrika *93*, 491–507. https://doi.org/10.1093/biomet/93.3.491.